Available online at www.sciencedirect.com
SCIENCE DIRECT®
International Journal of Thermal Sciences 45 (2006) 299–309
International Journal of Thermal Sciences
www.elsevier.com/locate/ijts

Numerical simulation of heat transfer during growth of single vapor bubbles in nucleate boiling

Petra Genske, Karl Stephan *

Institute of Technical Thermodynamics, University of Stuttgart, Pfaffenwaldring 9, D-70569 Stuttgart, Germany

Received 12 November 2003; received in revised form 1 July 2004; accepted 1 July 2004

Available online 10 October 2005

Abstract

In the model presented in this paper the region around a single growing vapor bubble in nucleate boiling is subdivided into three parts: a small, ring-shaped zone between heating wall and bubble, called micro-region, the bubble itself, and its surrounding liquid, referred to as macro-region.

As the micro-region is most important for heat transfer, a recently developed model put special emphasis on this region, and predicted heat transfer, bubble growth, and departure diameters of vapor bubbles for low to moderate heat fluxes fairly well.

The current paper aims at modeling the macro-region in more detail than done before. For this purpose, Navier–Stokes equations for both vapor and liquid phase were solved with the aid of a finite element method. It turned out that the flow pattern in the liquid around a growing vapor bubble is determined by the movement of the bubble surface, but also by the vapor flow inside the bubble. The fluid in the macro-region transports cooler liquid towards the wall, thus increasing the heat transfer significantly. In regions farther away from the bubble, heat conduction prevails. Buoyancy was found to be of small influence compared to forced convection.

Velocity and temperature fields, heat fluxes, bubble contours, and departure diameters were calculated for different fluids. The apparent contact angle is decisive for growth rate and departure diameter. Disturbances, caused by departing and ascending bubbles, are included into the calculations.

Keywords: Heat transfer; Fluid flow; Bubble growth; Boiling; Numerical simulation

1. Introduction

Though nucleate boiling is important in many technical processes its mechanism is still not well understood and thus subject of experimental and theoretical research.

As shown quite recently [1–4] a substantial part of heat is transferred in a very small, ring-shaped area between wall and bubble, the so-called micro-region, with heat fluxes of up to 10^7 W·m^{-2}.

The aim of the project presented in this paper is to improve the existing model. So far emphasis was laid on the heat transfer mechanism in the micro-region itself, whereas the macro-region was modeled in a simplified form. The fluid flow around and within the bubble is now modeled in more detail, and its influence on bubble growth and heat transfer is examined. Thus a better understanding of heat transfer in nucleate boiling will be achieved.

In our model a moving mesh enabled us to track the bubble surface exactly and to study fluid flow and heat transfer in and around the bubble in detail. We accepted the drawback that complete growth cycles cannot be calculated, all the more as bubble growth cycles were already simulated by Fujita, Dhir, and others [5,6].

2. Model

We consider a single vapor bubble growing at a horizontal heating wall, Fig. 1. The modeling region comprises the bubble, part of the surrounding liquid, and the adjacent wall. Interference of neighboring bubbles is neglected, an assumption justified for low to moderate heat fluxes, when the average distance between neighboring bubbles is relatively large.

* Corresponding author.
E-mail address: stephan@itt.uni-stuttgart.de (K. Stephan).

1290-0729/$ – see front matter
doi:10.1016/j.ijthermalsci.2004.07.008

Nomenclature

A	area	m^2
c_p	specific heat at constant pressure	$J{\cdot}kg^{-1}{\cdot}K^{-1}$
d	diameter	m
g	gravitational acceleration	$m{\cdot}s^{-2}$
K	curvature	m^{-1}
$\dot{M}$	mass flow	$kg{\cdot}s^{-1}$
N_B	bubble site density	m^{-2}
p	pressure	Pa
$\dot{Q}$	heat flow	W
r	radial coordinate	m
S	free surface position	
t	time	s
T	temperature	K
u	velocity	$m{\cdot}s^{-1}$
$\vec{x}$	coordinate vector	m
z	axial coordinate	m

Greek symbols

α	heat transfer coefficient	$W{\cdot}m^{-2}{\cdot}K^{-1}$
β	volume expansion coefficient	K^{-1}
γ	surface tension	$N{\cdot}m^{-1}$
δ	thermal boundary layer thickness	m
Δh_V	enthalpy of vaporization	$J{\cdot}kg^{-1}$
ΔT	temperature difference $T_W - T_{sat}$	K
φ_{app}	apparent contact angle	°
λ	thermal conductivity	$W{\cdot}m^{-1}{\cdot}K^{-1}$
ρ	density	$kg{\cdot}m^{-3}$
σ	surface stress	$N{\cdot}m^{-2}$
ξ_{ads}	adhesion radius	m

Subscripts

0	reference
dep	departure
micro	micro-region
n	normal direction
r	radial direction
sat	saturation
t	tangential direction
W	wall
z	axial direction

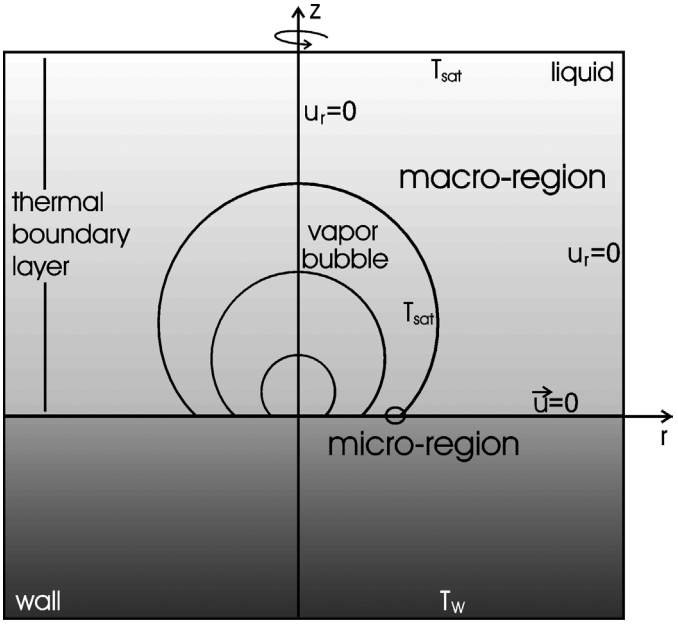

Fig. 1. Vapor bubble, surrounding liquid and adjacent wall with boundary conditions.

In previous calculations, concentrating on heat transfer in the micro-region, at each time step quasi-stationary heat conduction was assumed in the liquid surrounding the vapor bubble. The thermal boundary layer thickness was estimated by a Nusselt correlation for steady-state natural convection.

As emphasis in this work is on the macro-region, we investigate the effects of natural and forced convection flow around a growing bubble to determine its influence on heat transfer. The results from the previous micro-region model enter the macro-region model as boundary conditions.

2.1. Micro-region model

The flow and heat transfer in the wedge-shaped micro-region (located at the bubble foot) is described by mass, momentum, and energy balances together with equations for the liquid–vapor interphase geometry and saturation condition. The saturation temperature of the thin film varies because of the capillary forces due to curvature and adhesion forces between wall and liquid.

The model leads to a strongly non-linear system of four ordinary differential equations. Its solution yields the meniscus profile and the total heat flow transferred to the micro-region.

For a detailed discussion of the micro-region model please refer to [1,2], or [3].

2.2. Governing equations

Fluid flow in the liquid and in the vapor phase is described by equations of continuity, momentum, and energy, which read for an incompressible, laminar flow with constant properties in two-dimensional, axi-symmetric coordinates (see, e.g. [7]):

$$\frac{1}{r}\frac{\partial}{\partial r}(ru_r) + \frac{\partial u_z}{\partial z} = 0 \tag{1}$$

$$\rho\left(\frac{\partial u_r}{\partial t} + u_r\frac{\partial u_r}{\partial r} + u_z\frac{\partial u_r}{\partial z}\right) = -\frac{\partial p}{\partial r} + \mu\left(\frac{\partial}{\partial r}\left(\frac{1}{r}\frac{\partial}{\partial r}(ru_r)\right) + \frac{\partial^2 u_r}{\partial z^2}\right) \tag{2}$$

$$\rho\left(\frac{\partial u_z}{\partial t} + u_r\frac{\partial u_z}{\partial r} + u_z\frac{\partial u_z}{\partial z}\right) = -\frac{\partial p}{\partial z} + \mu\left(\frac{1}{r}\frac{\partial}{\partial r}\left(r\frac{\partial u_z}{\partial r}\right) + \frac{\partial^2 u_r}{\partial z^2}\right) + \rho g \tag{3}$$

$$\rho c_p\left(\frac{\partial T}{\partial t}+u_r\frac{\partial T}{\partial r}+u_z\frac{\partial T}{\partial z}\right)=\lambda\left(\frac{1}{r}\frac{\partial}{\partial r}\left(r\frac{\partial T}{\partial r}\right)+\frac{\partial^2 T}{\partial z^2}\right) \quad (4)$$

To allow for natural convection the Boussinesq approximation is employed. The varying density in the buoyancy term of the momentum equation is replaced by, see [7] for details:

$$\rho g=\rho_0\big(1-\beta(T-T_0)\big)g \quad (5)$$

All other fluid properties are assumed to be constant. Since temperature differences in nucleate boiling are small, results obtained with temperature-dependent properties hardly deviate from those calculated with constant properties.

In the heating wall we have heat conduction:

$$\rho c_p\frac{\partial T}{\partial t}=\lambda\left(\frac{1}{r}\frac{\partial}{\partial r}\left(r\frac{\partial T}{\partial r}\right)+\frac{\partial^2 T}{\partial z^2}\right) \quad (6)$$

Eqs. (1)–(6) were solved numerically with the commercial finite element program FIDAP, Fluent Inc., which uses a Galerkin-style finite element approach [8]. The resulting equations were solved either with a Newton–Raphson solver or a successive substitution. For simulation of the free surface a moving mesh was used. For numerical reasons calculations were carried out with dimensionless variables.

2.3. Geometry, initial and boundary conditions

We consider a two-dimensional, axi-symmetric geometry. The z-axis is placed in the bubble center, orthogonal to the wall, the r-axis parallel to the wall surface, Fig. 1. The size of the fluid region attributed to a single bubble is taken from experimental nucleation site density data [9,10]. As interference between neighboring bubbles is neglected, the bubble is assumed symmetrical. Symmetry boundary conditions are applied at both sides of the calculation region, i.e. no fluid flow and no heat flow across the boundary is allowed.

The height δ_T of the thermal boundary layer usually serves as upper boundary in z-direction, where constant temperature T_{sat} is assumed. The thickness $\delta_T=\lambda/\alpha$ for horizontal tubes of diameter d is calculated from

$$Nu=\frac{\alpha d}{\lambda}=\left\{0.60+\frac{0.387Ra^{1/6}}{[1+(0.559/Pr)^{9/16}]^{8/27}}\right\}^2 \quad (7)$$

For horizontal discs of diameter d it is determined from

$$Nu=\frac{\alpha L}{\lambda}=0.15Ra^{1/3}\left[1+\left(\frac{0.322}{Pr}\right)^{11/20}\right]^{-20/33}$$
$$L=\frac{d}{4} \quad (8)$$

Both correlations are taken from [11].

As usual the fluid velocity at the solid wall is assumed to be zero. This boundary condition is slightly modified for free surface calculations. Then a slip is assigned to a small part of the wall-near fluid allowing motion of the bubble foot. When the heating wall is not included in the calculations, a constant temperature T_W is appointed at the interphase between wall and fluid. In all other cases T_W is attributed to the inside of the heated wall.

The vapor phase and the bubble surface are assumed to be at saturation temperature T_{sat}. In the macro-region mass transfer across the interphase is neglected. For natural convection simulations a slip is assumed to exist at the bubble surface, i.e. only tangential flow, but no fluid flow normal to the surface is permitted. In free surface flow simulations the interphase is allowed to move. This will be explained in detail in the respective section of this paper.

Due to mesh limitations, simulations have to start with a small initial bubble. Its geometry and the corresponding starting time were determined from calculations done with the previous micro-region model.

Realistic for the first bubble developing at a nucleation site and for sufficiently long waiting periods between bubbles, as well, is the initial assumption of a quiescent fluid and linear temperature distribution within the thermal boundary layer. If waiting periods are short, fluid flow in the wake of the departing bubble will change these initial conditions. Fluid flow and temperature field disturbance by a departing bubble for this case were calculated separately, and then served as initial conditions for the following bubble. This will be explained in detail in the respective section.

3. Natural convection

Steady-state simulations with stationary bubble contours were conducted with different fluids, different heating wall materials and various bubble diameters. As an example, Fig. 2 presents results for i-pentane at $p=0.333$ MPa ($p^*=0.1$). Results for R114 were published elsewhere [12,13].

Fig. 2(a) visualizes two flow areas that have developed in the liquid. In the vicinity of the bubble liquid from the bulk flows towards the wall, initiated by the lower temperature of the bubble surface. Farther away, a secondary natural convection flow circulation develops.

The flow changes the initially linear temperature field in the fluid, clearly visible in Fig. 2(b) above the bubble and in the middle section. Maximum velocities are about 0.9 mm·s^{-1}, which is still slow compared to the average bubble growth velocity of about 26 mm·s^{-1}, as it was calculated with the micro-region model [1] in good agreement with experimental data [10].

In general, natural convection velocities turn out to be roughly one order of magnitude smaller than forced convection velocities estimated from bubble growth rates. Natural convection influence thus is expected to be small. It is superimposed by strong forced convection flow caused by the growing bubble.

4. Influence of displacement forces

When the bubble grows, its expanding surface displaces the surrounding liquid, according to

$$\vec{u}_{\text{Fluid}}=\vec{u}_{\text{Surface}} \quad (9)$$

at the interphase. The surface velocity $\vec{u}_{\text{Surface}}$ could be taken

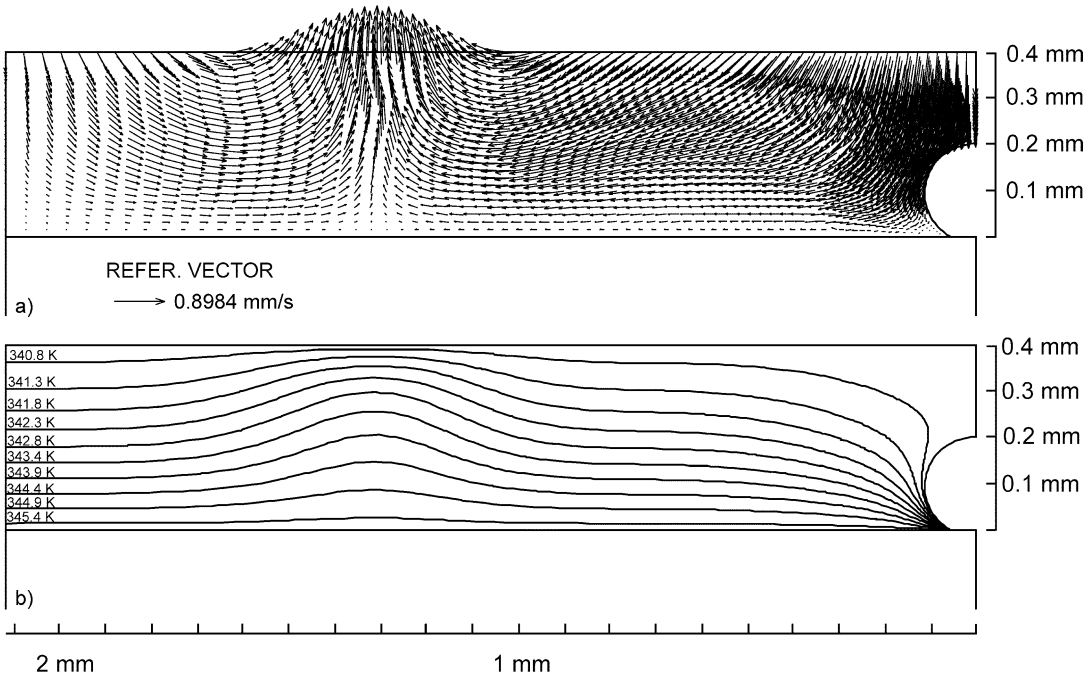

Fig. 2. Natural convection. Velocities and isotherms around a stationary bubble; i-pentane, $p = 0.333$ MPa, $\Delta T = 5.2$ K, $N_B = 7\ \mathrm{cm}^{-2}$.

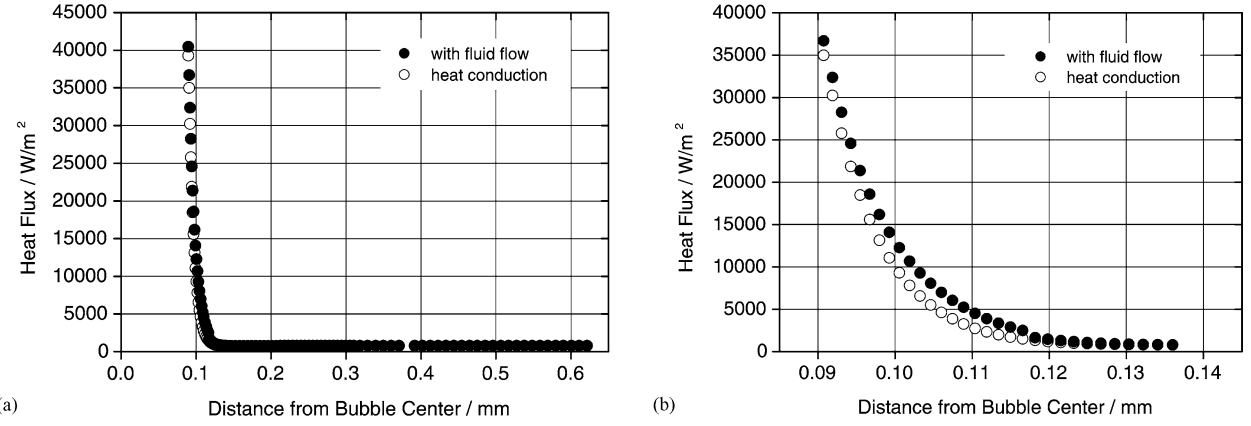

Fig. 3. Heat fluxes from wall to liquid in the macro-region after 0.0078 s; R114, $p = 0.247$ MPa, $\Delta T = 4$ K. Displacement flow compared to pure heat conduction.

from bubble growth rates of the previous micro-region model because of the good agreement with experimental data [1], even though fluid flow in the macro-region was neglected in these previous calculations.

A specific velocity and direction was appointed to each mesh point on the moving bubble surface. The vapor phase was assumed to be homogeneous and of constant temperature, and fluid flow in the vapor was neglected.

Selected results are presented. Results obtained for R114 with this approach were published in [13].

In Fig. 3(a) heat fluxes from wall to liquid in the macro-region are plotted for a fixed time step over the distance from the bubble center. Throughout most part of the macro-region the heat flux is constant and relatively low. Close to the bubble surface, when approaching the micro-region, it increases rapidly. Within the micro-region, which is not included in the diagram, it reaches values above $10^6\ \mathrm{W{\cdot}m^{-2}}$. Fig. 3(b) illustrates the small difference between the heat fluxes when fluid

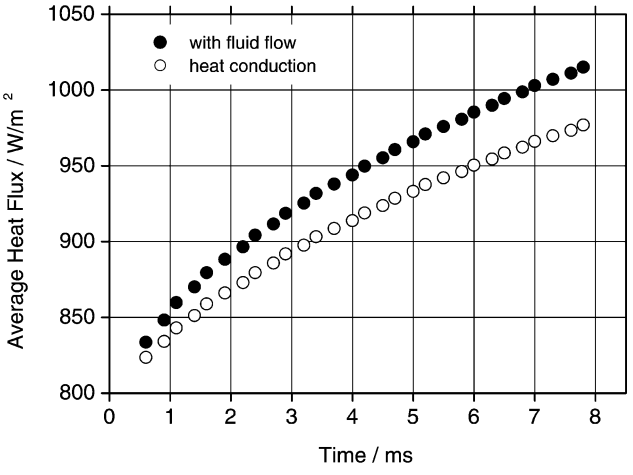

Fig. 4. Heat fluxes from wall to liquid; R114, $p = 0.247$ MPa, $\Delta T = 4$ K. Displacement flow compared to pure heat conduction.

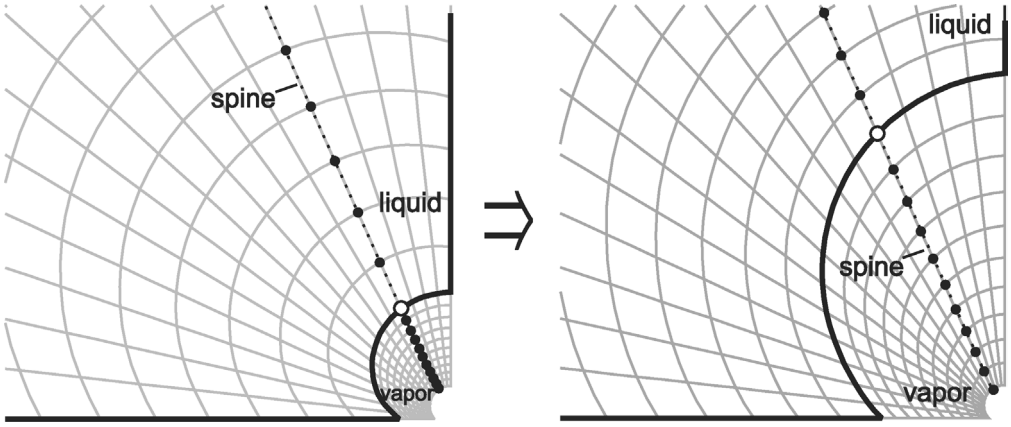

Fig. 5. Nodes moving along a spine when the bubble surface expands.

flow is taken into account and when pure heat conduction is assumed.

Fig. 3(a) and (b) clearly show that fluid flow caused by displacement forces has almost no influence on heat flux from wall to liquid. Only near the bubble surface, where fluid flow is strongest, an increase of heat flow is noticed.

Fig. 4 depicts the average heat flux as a function of time. Due to the relatively small area of increased heat transfer the average heat flux in the micro-region increases by only approximately 3%.

As a result we note that fluid flow due to displacement forces alone hardly increases heat transfer at all.

5. Free surface simulation

In the following the governing equations will be solved in both vapor and liquid phase. The position of the interface between the two phases is treated as an additional degree of freedom and is determined at each time step.

Determination of the position of the free surface $S(\vec{x},t)$ requires additional equations to be included in the model:

$$\frac{\partial S}{\partial t}+u_r^{(1)}\frac{\partial S}{\partial r}+u_z^{(1)}\frac{\partial S}{\partial z}=\frac{\partial S}{\partial t}+u_r^{(2)}\frac{\partial S}{\partial r}+u_z^{(2)}\frac{\partial S}{\partial z}=0 \quad (11)$$

$$\sigma_n^{(1)}-\sigma_n^{(2)}=2\gamma K \quad (12a)$$

$$\sigma_t^{(1)}-\sigma_t^{(2)}=-\vec{t}\cdot\nabla\gamma=0 \quad (12b)$$

$$\left(\vec{u}^{(1)}-\vec{u}^{(2)}\right)\cdot\vec{t}=0 \quad (13)$$

with tangent vector $\vec{t}$, (1) and (2) denoting liquid and vapor. Eq. (11) is the governing equation of the surface position $S(\vec{x},t)$, Eq. (12) and (13) are the boundary conditions to be fulfilled at the free surface.

Whereas in pure liquids the variation of surface tension γ with temperature is small and can be neglected, in mixtures its dependence of concentration has to be taken into account [14].

During the simulation, the bubble surface mesh points are allowed to move along certain lines, so-called spines, Fig. 5. Thus the exact position of the free surface is known at each time step.

With the above model of the free surface a quite detailed examination of fluid flow in both vapor and liquid phase, as well as heat transfer in the vicinity of the growing bubble can be determined. Liquid flow is not only initiated by displacement forces, but also influenced by the vapor flow inside the bubble, mostly neglected in previous studies.

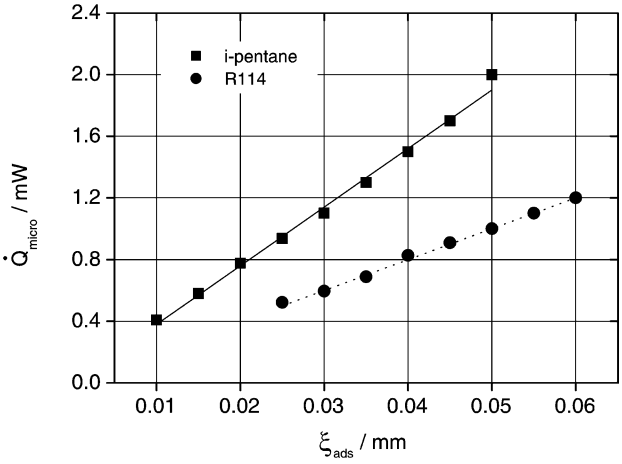

Fig. 6. Micro-region heat flow.

5.1. Vapor inflow

Liquid evaporates mainly in the micro-region, while vaporization along the bubble surface in the macro-region is comparatively small. From the micro-region model we obtain the velocity of vapor entering the bubble, which serves as a boundary condition for our macro-region simulation. As heat flow depends on the adhesion radius ξ_{ads} of the bubble, the inflow velocity is a function of ξ_{ads} and as such incorporated into our model.

In Fig. 6 micro-region heat flows $\dot{Q}_{Micro}$, calculated with the micro-region model (see [1]), are plotted for two different fluids. As $\dot{Q}_{Micro}$ increases almost linearly with ξ_{ads}, a linear function was used in our simulation to determine $\dot{Q}_{Micro}$ for each bubble adhesion radius in the growth cycle. From the mass flow

$$\dot{M}_{Micro}=\dot{Q}_{Micro}/\Delta h_V \quad (14)$$

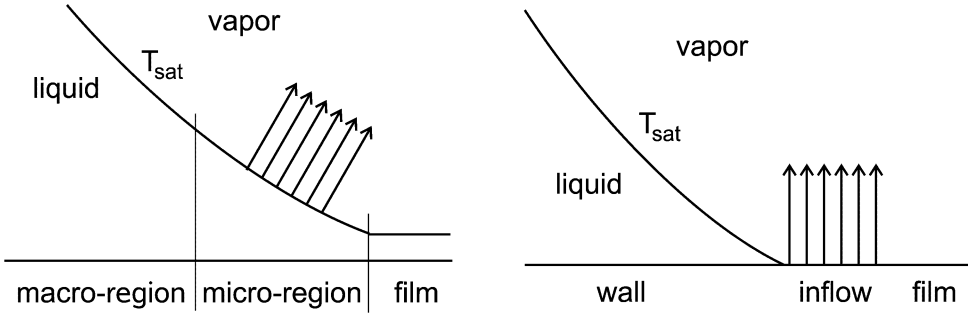

Fig. 7. (a) Actual micro region inflow; (b) Inflow region used for the calculations.

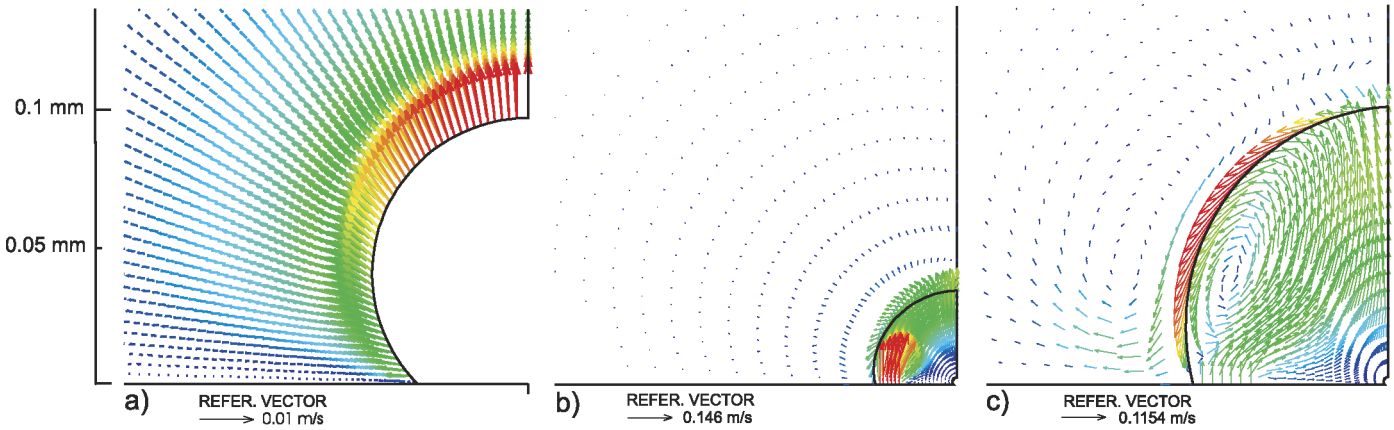

Fig. 8. Flow pattern in and around growing bubbles; R114, $p = 0.247$ MPa, $\Delta T = 4$ K, $N_B = 81$ cm^{-2}; (a) Forced convection due to displacement forces; (b), (c) Free surface results.

we then obtain the vapor inflow velocity

$$u_{z,\text{inflow}} = \dot{M}_{\text{Micro}} / \rho_V A_{\text{Micro}} \tag{15}$$

Fig. 7(a) shows the actual vapor inflow, and Fig. 7(b) the inflow region as it was modeled. As Fig. 7(b) shows, the inflow section in the model is placed directly at the wall, not taking into account the thin layer of liquid in the micro-region.

5.2. Flow inside and around a growing bubble and its influence on heat transfer

Within the bubble the inflowing vapor rises in the center and streams down along the bubble surface. At the beginning, the displacement of the surrounding liquid by the growing bubble gives rise to a liquid flow normal to the bubble surface, Fig. 8(b), similar to the flow pattern that develops if only displacement forces are considered, Fig. 8(a).[1] When the bubble continues to grow, circulation of vapor inside the bubble develops, and the liquid close to the bubble starts to flow downwards along the surface, Fig. 8(c). A second circulating flow is developing in the liquid, transporting cooler liquid towards the wall, thereby increasing heat transfer in that area significantly.

As an example, free surface calculation results for R114 at $p = 0.247$ MPa and $\Delta T = 4$ K at two time steps are presented in Figs. 9–11.

After 4 ms the bubble is already close to departure. The flow pattern is fully developed, Fig. 9. Vapor circulates inside the bubble, and liquid flows downwards along the bubble surface, forming an eddy-like pattern near the bubble base. Thereby cooler liquid is transported towards the wall. The area of cooler liquid is clearly visible in Fig. 10. In this area heat transfer distinctly increases compared to pure heat conduction, Fig. 11, while in areas apart from the bubble the influence of fluid flow is negligible.

The behavior depicted in Figs. 9–11 is typical for all fluids examined so far. Fig. 12 shows respective temperature fields in *i*-pentane.

5.3. Influence of departing bubbles on heat transfer

So far a linear temperature field in a quiescent fluid was assumed initially. This is realistic for the first bubble to develop at a nucleation site, and for long waiting periods between bubbles. The growing and departing bubble initiates, however, the temperature and velocity field for the next bubble.

In order to study this effect, three separate simulations were undertaken. As step one, a growing bubble was simulated, and the calculation was stopped shortly before bubble departure. In step two, a circular bubble of fixed shape and departure diameter was modeled in a separate simulation. In this

[1] Figs. 8–10, 12, and 13 are presented in colour in the electronic form of the paper in Science direct.

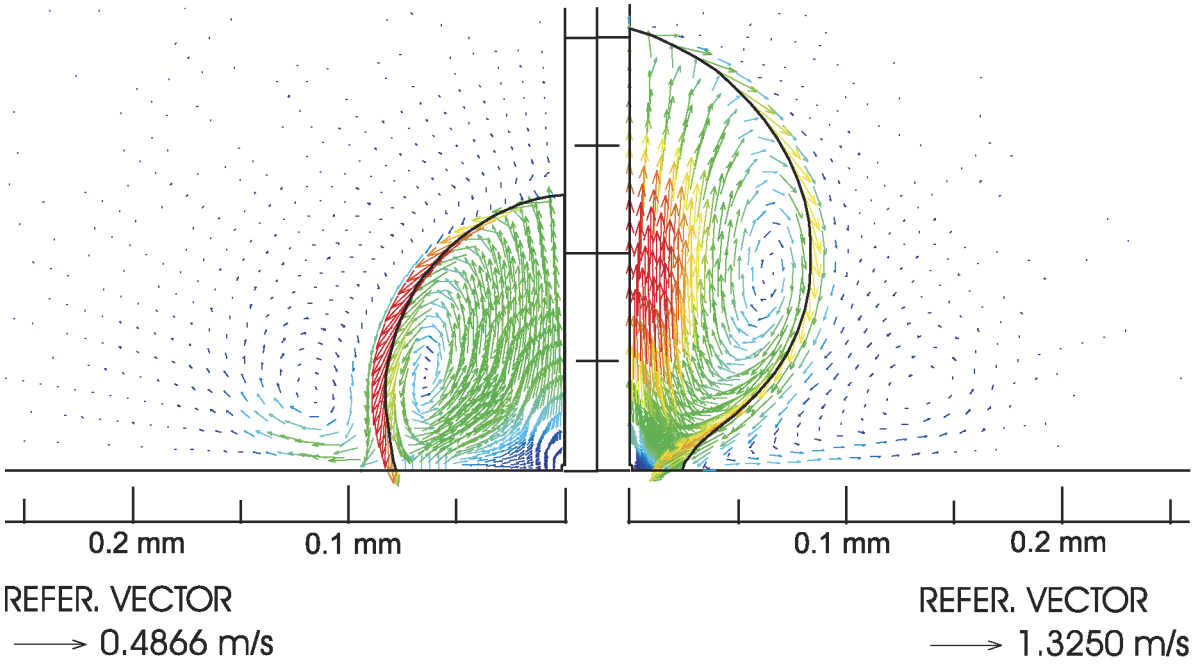

Fig. 9. Velocity field around and inside a growing vapor bubble after 3 ms (left) and 4 ms (right). R114, $p = 0.247$ MPa, $\Delta T = 4$ K, $N_B = 81$ cm^{-2}.

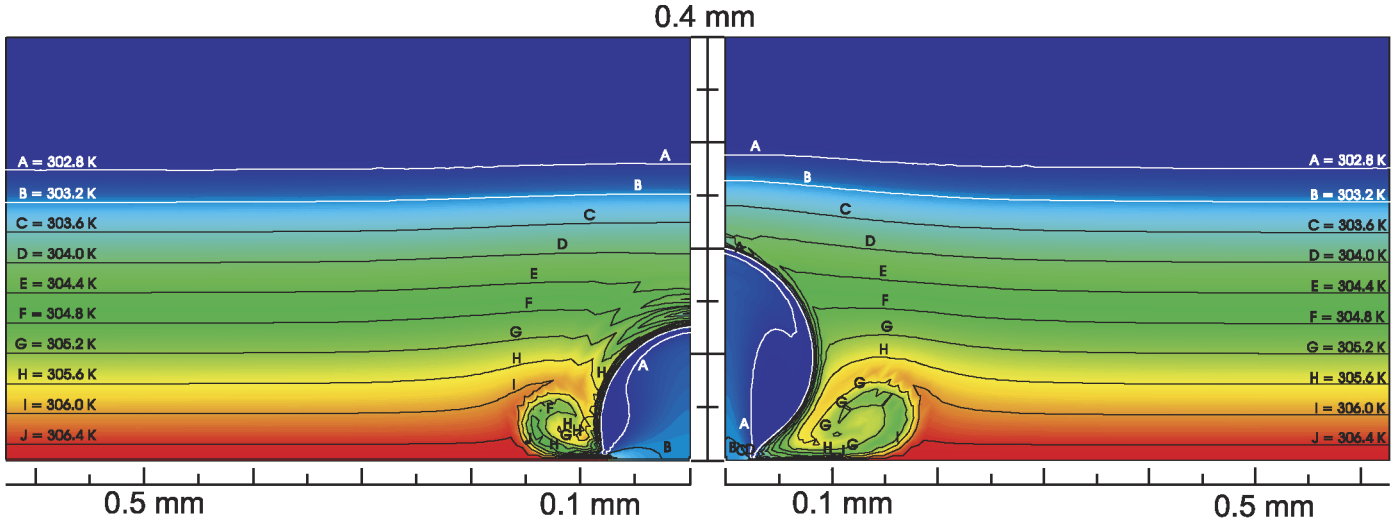

Fig. 10. Temperature field around and inside a growing vapor bubble after 3 ms (left) and 4 ms (right). R114, $p = 0.247$ MPa, $\Delta T = 4$ K, $N_B = 81$ cm^{-2}.

simulation, the temperature and velocity fields around the almost departed first bubble were used as initial condition for the ascending bubble. A constant upward velocity was appointed to the bubble, based on the terminal velocity [15]. When the ascending bubble had gained some distance from the wall, the simulation was stopped. The resulting temperature and velocity fields were saved, and, in a third step, used as initial conditions for the next bubble growth simulation.

While the model of the ascending bubble is fairly simplified, we nevertheless get a good guess on how much forced convection flow caused by departing and ascending bubbles influences heat transfer from wall to liquid. These effects lead to a further increase of heat transfer in the macro-region.

In Fig. 13(a) the resulting temperature fields are depicted. The ascending bubble simulation was carried out for 5 ms; afterwards the resulting temperature and velocity fields were used as initial conditions. After 0.5 ms, when the new growing bubble is still small, the effects which the previous bubble had on the temperature distribution are clearly visible. The new bubble develops in an area of warm fluid swept upwards in the wake of the departing bubble, and surrounded by cooler liquid from the bulk that flew down to fill the void. The area of cooler liquid near the wall, developed during the growth period of the previous bubble, Fig. 10, is still present. After 4 ms, Fig. 13(b), we notice still a volume of warmer liquid above the bubble. As before, Fig. 10, downward flowing liquid transported cooler fluid towards the bubble base. As the liquid in the bulk above the

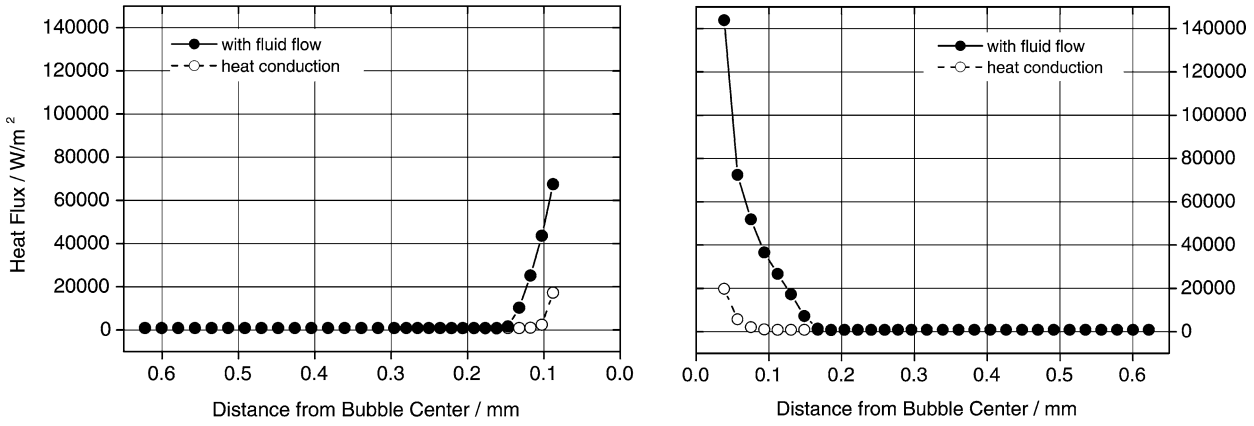

Fig. 11. Heat flux from wall to liquid compared to pure heat conduction fluxes after 3 ms (left) and 4 ms (right). R114, $p = 0.247$ MPa, $\Delta T = 4$ K, $N_B = 81$ cm^{-2}.

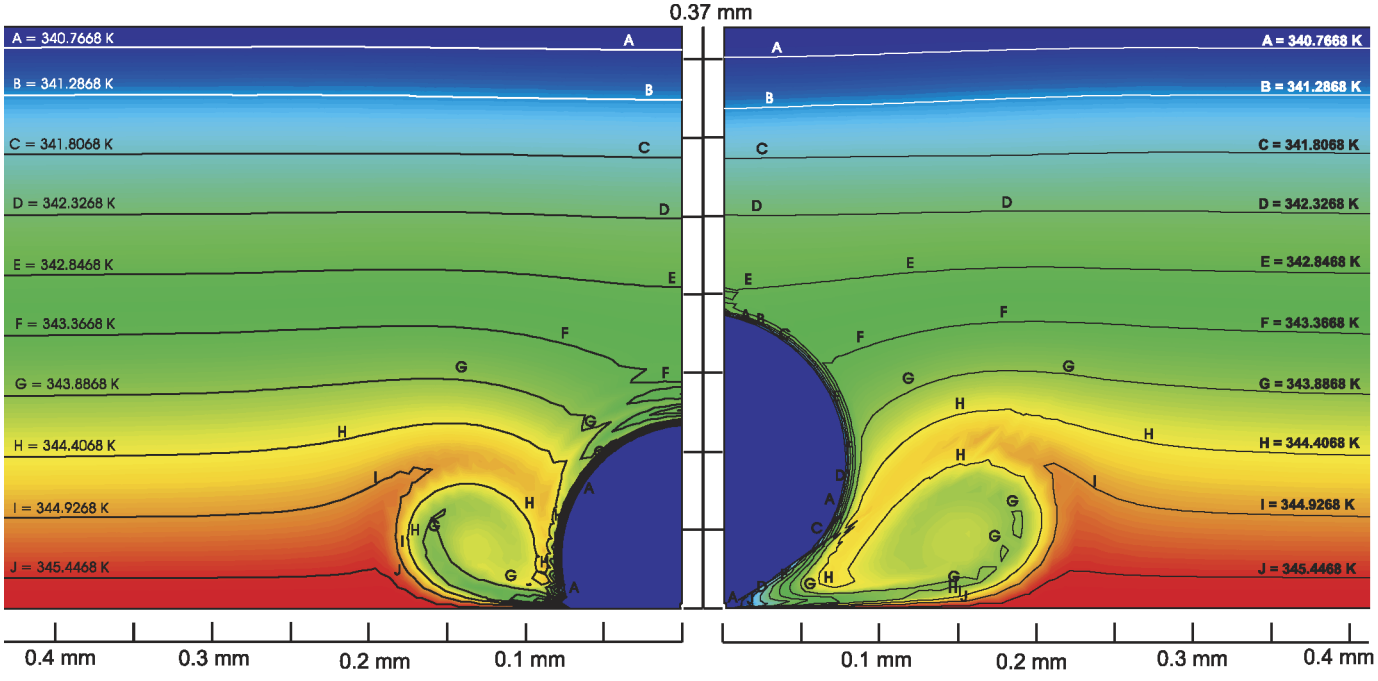

Fig. 12. Temperature field around and inside a growing vapor bubble after 4.5 ms (left) and 5.79 ms (right). *i*-pentane, $p = 0.333$ MPa, $\Delta T = 5.2$ K, $N_B = 7$ cm^{-2}.

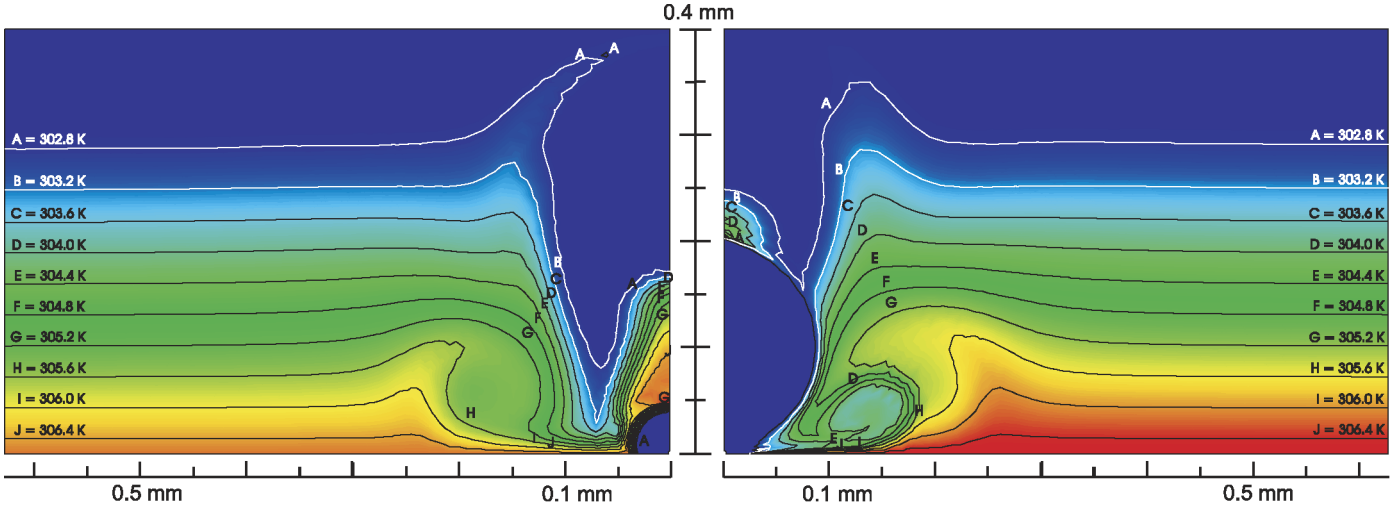

Fig. 13. Temperature field after 0.5 and 4 ms. Departing bubbles taken into account. R114, $p = 0.247$ MPa, $\Delta T = 4$ K, $N_B = 81$ cm^{-2}.

bubble is cooler, this area is of lower temperature than before, which causes an additional increase in heat transfer.

A comparison of calculated temperature and velocity fields with experimental results is difficult, as such measurements are not easy to undertake in the direct vicinity of so small a bubble. In [16] Buchholz and Auracher describe their experimental measurement of temperatures very close to and 9 mm above a horizontal heating wall in nucleate boiling of isopropanol. Liquid overheats of several K were found close to vapor bubble boundaries. Such effects could be explained by superheated liquid that is swept along in the wake of a departing bubble, as visible in Fig. 13(a). A direct comparison of results is difficult, though, as the heat fluxes in [16] are a lot higher than those used in our simulations.

5.4. Heat transfer in the vicinity of a growing bubble

The area around a vapor bubble can be subdivided into four sections with different heat transfer mechanisms, Fig. 14. In previous works two major areas were named, the micro-region and the macro-region. The micro-region consists of two sections, the adsorbed film (I) and the actual micro-region (II). Heat transfer in the film area (I) almost disappears, while in the micro-region (II) heat fluxes are highest [1–4].

The results presented in this paper suggest dividing the macro-region into two sections, as well. Close to the bubble we have an area where heat transfer increases significantly due to fluid flow (III), clearly visible in Figs. 10–12. For the fluids examined this area stretches up to roughly 0.1 mm to 0.2 mm beyond the bubble base into the macro-region. Farther apart, in section (IV), heat conduction prevails and fluid flow can be neglected (IV).

Fluid flow is of considerable influence on heat transfer. Cooler liquid flows towards the wall and leads to a considerable increase of heat fluxes, becoming larger when the bubble grows. In a pure heat conduction environment heat flow would remain almost constant over the bubble growth period.

As the example of R114 shows, Fig. 15, the heat flow in the macro-region increases steadily during bubble growth. When the bubble comes close to departure and the bubble base constricts, an additional increase in heat flow is noted. The micro-region heat flow increases as long as the adhesion radius grows, then decreases when the adhesion radius becomes smaller and vanishes with bubble departure.

An additional increase in macro-region heat flow is noted that comes from the flow field induced by departing bubbles. Fig. 15 shows the deviation between heat flows around bubbles that grow in an initially quiescent fluid, marked as circles, and bubbles that grow in a fluid disturbed by previously ascending bubbles, marked as squares. During the first part of the simulation the deviation becomes slightly smaller, as cooler liquid transported towards the wall during the growth period of the previous bubble is slowly heated again. After a certain time, when fluid flow around the new growing bubble has fully developed, the deviation between the heat flows remains almost constant until the end of the simulation.

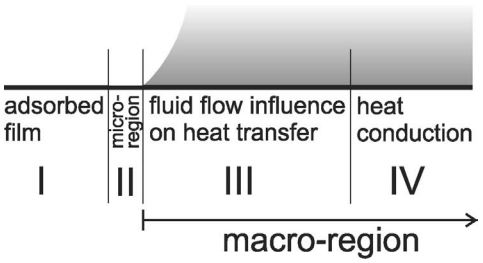

Fig. 14. Areas in which different heat transfer mechanisms prevail.

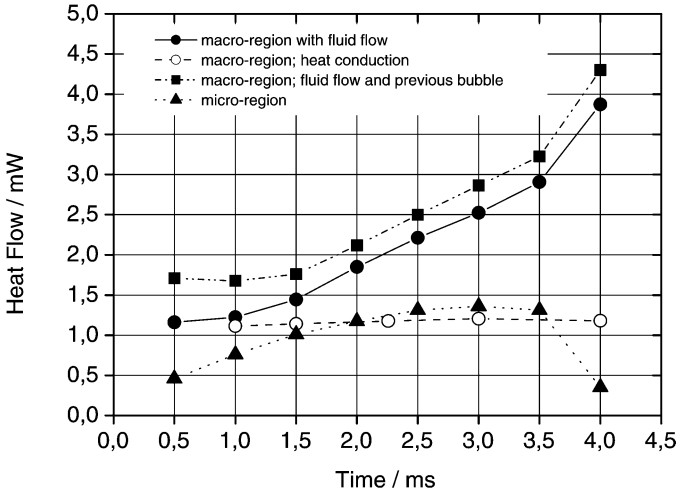

Fig. 15. Macro- and micro-region heat flows plotted against time. R114, $p = 0.247$ MPa, $\Delta T = 4$ K, $N_B = 81$ cm^{-2}.

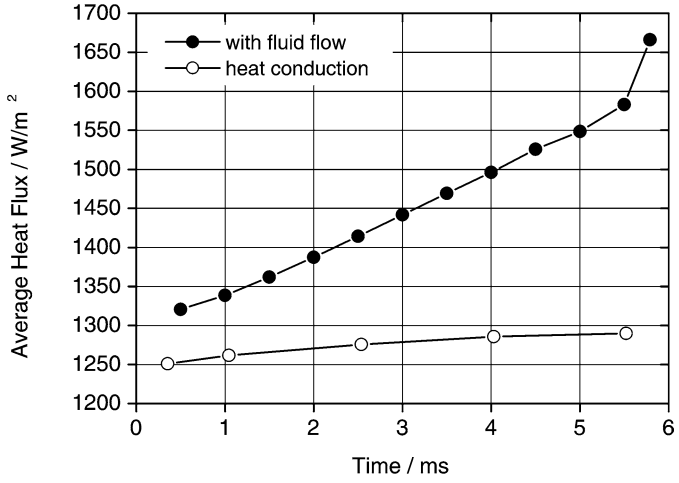

Fig. 16. Macro-region heat fluxes. i-pentane, $p = 0.333$ MPa, $\Delta T = 5.2$ K, $N_B = 7$ cm^{-2}.

Similar results were found for i-pentane, Fig. 16. During bubble growth average macro-region heat fluxes increase almost linearly with time, with a strong additional increase shortly before bubble departure.

Nucleate boiling heat transfer around horizontal tubes was studied by Mann [1]. He identified the following heat transfer mechanisms: vaporization, heat transfer around attached bubbles, heat transfer initiated by bubbles ascending along the tube, and free convection.

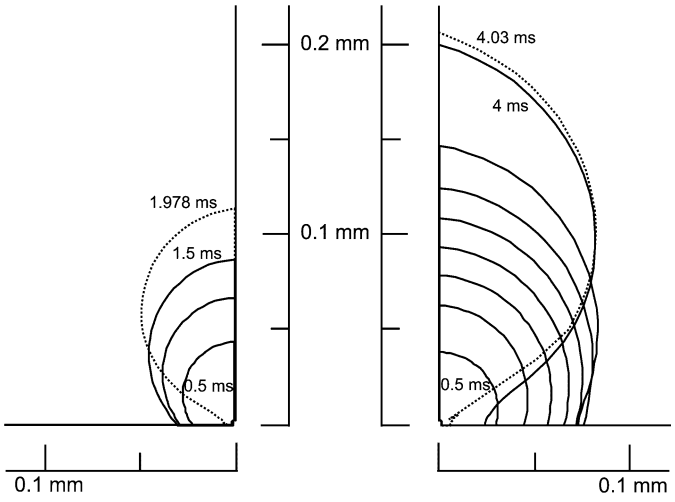

Fig. 17. Bubble growth contours and departure diameter (dashed line) for two different apparent contact angles. Left: 55°, right: 75°. R114, $p = 0.247$ MPa, $\Delta T = 4$ K.

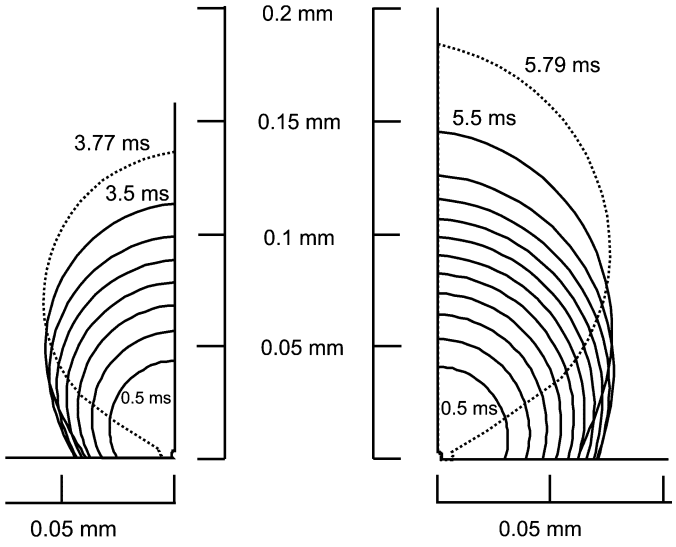

Fig. 18. Bubble growth contours and departure diameter (dashed line) for two different apparent contact angles. Left: 65°, right: 75°. *i*-pentane, $p = 0.333$ MPa, $\Delta T = 5.2$ K.

For R114 he calculated a heat transfer coefficient of 1220 $W{\cdot}m^{-2}{\cdot}K^{-1}$, of which 587 $W{\cdot}m^{-2}{\cdot}K^{-1}$ are due to vaporization, the rest is caused by convection. According to our model the convective flow at the bubble base is of influence, as well. If we add it to the convective part of the heat transfer coefficient determined by Mann, we find an overall heat transfer coefficient of 1355 $W{\cdot}m^{-2}{\cdot}K^{-1}$, which is higher than the value of Mann, but still around 20% below the experimental value found by Barthau [9].

5.5. Bubble contours and contact angle

In Fig. 17 and 18 bubble contours at different time steps are depicted for R114 and *i*-pentane. After a relatively long period during which the bubble adhesion zone is growing, we find a short stagnation period, followed by a rapid detachment process. Then the adhesion radius shrinks, and the bubble volume moves upwards. Due to mesh limitations our simulations stopped shortly before the actual departure.

Different apparent contact angles were chosen for the calculations. It should be noticed that these apparent contact angles are larger than the apparent contact angles that would be obtained at the end of the micro-region. As apparent contact angles increase rapidly with distance from the micro-region, they strongly depend on the position where they are taken.

For R114, with an apparent contact angle of 75° a departure diameter of 0.21 mm was calculated, fairly close to the experimental value of 0.25 mm [9], Fig. 17. For *i*-pentane with the same apparent contact angle, the deviation between the predicted diameter of 0.18 mm and the average measured departure diameter of 0.3 mm [10] is larger, Fig. 18.

For all fluids considered the time at which detachment begins, and thus the departure diameter, strongly depends on the apparent contact angle. The larger the apparent contact angle, the later starts detachment, and the larger the bubbles become before departure, Fig. 19. Similar results were already found for water by Dhir [6].

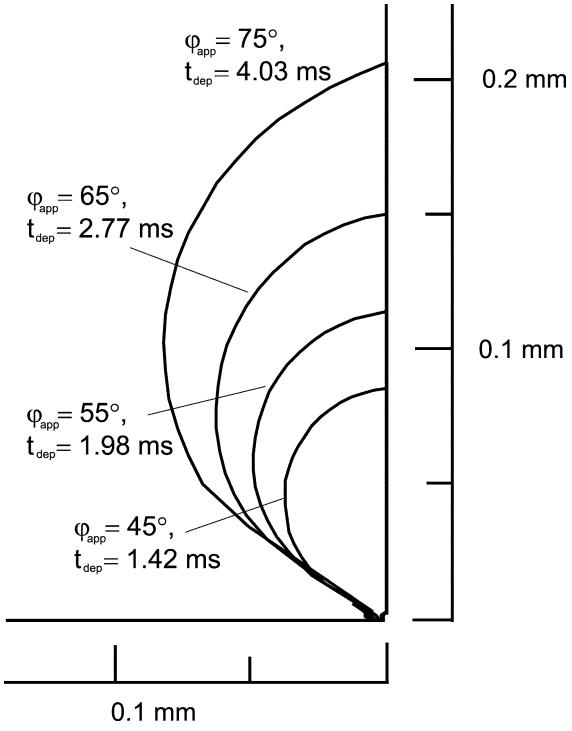

Fig. 19. Departure diameters for different apparent contact angles. R114, $p = 0.247$ MPa, $\Delta T = 4$ K.

6. Summary

A growing vapor bubble and its surrounding liquid were modeled and simulated for two different fluids (R114, *i*-pentane). The aim of the project was to gain a better understanding on how forced convection flow initiated by the growing bubble influences heat transfer.

Micro-region heat flows predicted with a separate model were used to calculate the velocity of vapor flowing into the bubble. During bubble growth, velocities and temperature dis-

tribution in both vapor and liquid were determined and resulting heat fluxes calculated.

A small region in the vicinity of the bubble (in the cases examined a zone 0.1 to 0.2 mm wide) was found in which fluid flow leads to a significant increase of heat transfer, while in areas farther away from the bubble heat conduction prevails. Thus the macro-region, i.e. the liquid around the bubble, can be subdivided into two areas with different heat transfer characteristics: A smaller area close to the bubble, in which forced convection flow has a strong influence on heat transfer, and an area, in which heat conduction prevails. The size of this area depends on bubble site density. At low heat fluxes it is much larger than the area in which forced convection prevails.

Displacement forces, causing only radial liquid movement, resulted in heat fluxes only slightly larger than those of heat conduction. In reality the interaction between vapor and liquid flow at the interphase leads to a strong increase in heat transfer. Fluid from the bulk then flows downwards along the bubble surface, transporting cooler liquid towards the heating wall, and thereby increasing the heat transfer.

Bubble growth contours and departure diameters were determined, as well. Departure time and diameters strongly depended on the apparent contact angle. The larger the apparent contact angle, the larger the break-off volume of the bubble.

Acknowledgement

The authors highly appreciate financial support of Deutsche Forschungsgemeinschaft (DFG) in the frame of a joint research project on fundamentals of boiling heat transfer, and thank all members of the joint research project for their cooperation and valuable discussions.

References

[1] M. Mann, Ein Mikrozonenmodell zur Beschreibung der Blasenbildung und des Wärmeübergangs beim Sieden, PhD thesis, University of Stuttgart, Stuttgart, Germany, 2001.

[2] J. Hammer, Einfluss der Mikrozone auf den Wärmeübergang beim Blasensieden, PhD thesis, University of Stuttgart, Stuttgart, Germany, 1996.

[3] P. Stephan, J. Hammer, A new model for nucleate boiling heat transfer, Wärme- und Stoffübertragung 30 (1994) 119–125.

[4] P. Stephan, J. Hammer, The role of micro-region phenomena on nucleate boiling, in: 2nd European Thermal Science and 14 UIT National Heat Transfer Conference, Rome, Italy, 1996.

[5] Q. Bai, Y. Fujita, Numerical simulation of the growth for a single bubble in nucleate boiling, Thermal Sci. Engrg. 7 (1999) 45–53.

[6] V.K. Dhir, Numerical simulations of pool boiling heat transfer, AIChE J. 47 (2001) 813–834.

[7] R.B. Bird, W.E. Stewart, E.N. Lightfoot, Transport Phenomena, second ed., Wiley & Sons, New York, 2002.

[8] FIDAP, FIDAP V8.6, Fluent Inc., Lebanon, USA, 2001.

[9] G. Barthau, Active nucleation site density and pool boiling heat transfer—an experimental study, Internat. J. Heat Mass Transfer 35 (1992) 271–278.

[10] M. Weckesser, Untersuchungen zur Blasenbildung beim Sieden in freier Konvektion, PhD thesis, University of Karlsruhe, Karlsruhe, Germany, 1990.

[11] H.D. Baehr, K. Stephan, Wärme- und Stoffübertragung, fourth ed., Springer, Berlin, 2003.

[12] P. Genske, K. Stephan, Nucleate boiling—Numerical simulation of heat transfer at moderate heat fluxes, in: Proceedings of the International Institute of Refrigeration Conference, Commission B1, Thermophysical Properties and Transfer Processes of New Refrigerants, October 3–5, 2001, Paderborn, Germany.

[13] P. Genske, K. Stephan, Numerical simulation of heat transfer during growth of vapor bubbles in nucleate boiling, in: Proceedings of the 12th International Heat Transfer Conference, August 18–23, 2002, Grenoble, France.

[14] J. Kern, P. Stephan, Assessment of a theoretical model for the nucleate boiling heat transfer coefficient of binary mixtures, in: Proceedings 3rd European Thermal Sciences Conference, vol. 2, Edizioni ETS, Heidelberg, 2000, pp. 779–784.

[15] R. Clift, J.R. Grace, M.E. Weber, Bubbles, Drops, and Particles, Academic Press, New York, 1978.

[16] M. Buchholz, H. Auracher, T. Lüttich, W. Marquardt, A study of local heat transfer mechanisms along the entire boiling curve by means of microsensors, Int. J. Thermal Sci. 45 (3) (2006) 269–283 (this issue).